

Delay time and Non-Adiabatic Calibration of the Attoclock

Multiphoton process versus tunneling in strong field interaction

Ossama Kullie

Theoretical Physics, Institute for Physics, Department of Mathematics
and Natural Science, Universität Kassel, 34132 Kassel, Germany*

Igor Ivanov

Center for Relativistic Laser Science, Institute for Basic Science (IBS), Gwangju 61005, Republic of Korea

The measurement of the tunneling time in attosecond experiments, termed attoclock, triggered a hot debate about the tunneling time, the role of time in quantum mechanics, where the interaction with the laser pulse involves two regimes of a different character, the multiphoton and the tunneling (field-) ionization. In the adiabatic field calibration, one of us (O. K.) developed in earlier works a real tunneling time model and showed that the model fits well to the experimental data of Landsmann et al. (Optica **1**, 343 2014). In the present work, it is shown that the model explains the experimental result in the nonadiabatic field calibration, where one reaches a good agreement with the experimental data of Hofmann et al. (J. of Mod. Opt. **66**, 1052, 2019). Furthermore, we confirm the result with the numerical integration of the time-dependent Schrödinger equation. The model is appealing because it offers a clear picture of the multiphoton and tunneling field-ionization regimes. In the nonadiabatic case (the nonadiabatic field calibration), the ionization is mainly driven by multiphoton absorption. Surprisingly, at a field strength $F \leq F_a$ (F_a is the atomic field strength) the model always predicts a time delay with respect to the quantum limit τ_a at $F = F_a$. For an adiabatic tunneling, the saturation at the limit ($F = F_a$) explains the well-known Hartman effect or Hartman paradox.

Keywords: Ultrafast science, attosecond physics, attoclock, strong field approximation, multiphoton processes, tunneling and field-ionization time delay, nonadiabatic effects, time-energy uncertainty relation, Hartman paradox.

I. INTRODUCTION

The measurement of the tunneling time, in the strong field laser-matter interaction and attosecond science, triggered a hot debate about the tunneling with its adiabatic and nonadiabatic frontiers, the multiphoton and the intermediate regimes, the tunneling time and the role of time in quantum mechanics. Tunneling happens when the interacting electron is field-ionized by a tunneling mechanism, which can occur when the field strength of the laser pulse is strong enough but smaller than the atomic field strength F_a of the system (an atom or a molecule). F_a is defined by the ionization potential of the valence or the interacting electron. In the adiabatic tunneling, Kullie presented in a previous work [1] a tunneling model, in which the tunneling time (T-time) is a time delay with respect to ionization time at atomic field strength F_a . The tunneling time delay showed a good agreement with the attoclock result or the attosecond (angular streaking) experiment of Landsmann et al. [2–4] for Helium (He-) atom [1], and of Sainadh et al. [5] for Hydrogen (H-) atom [6] (apart from a factor 1/2) and with the accompanying numerical integration of the Schrödinger equation (NITDSE) of [5]. Furthermore, the T-time picture of [1] shows an intriguing similarity to the famous Bohr-Einstein weighing *photon box Gedanken experiment (BE-photon-box-GE)* [7], [8] (p. 132), where the former can be considered as a realization of the latter.

The description of the tunneling ionization process which we propose differs from the traditional approach based on the evaluation of the expression for the ionization amplitude obtained by using the saddle point method (SPM). Such an approach leads ultimately to the well-known imaginary time (ITM) [9, 10] and quantum orbit (QO) [11, 12] methods, which offer the following interesting and appealing picture of the ionization process. An electron trajectory (generally complex) originates at the (complex) moment of time corresponding to the saddle point, descends further on the real time-axis, and propagates in the real time after intercepting the real time-axis. The real part of the complex saddle point can be interpreted as the moment when the electron begins the under-the-barrier motion (hence the complex-valued time and velocity),

and the point of intercept of the quantum trajectory with the real time-axis as the moment of time when the electron exits the tunneling barrier or the time when the ionization event occurs. This picture proved to be extremely useful in understanding the tunneling ionization process. We should note, however, that it is no means unique description of the tunneling ionization. Indeed, the description based on the SPM and complex quantum trajectories is but convenient way to visualize ionization process. This can be seen already from the fact, that the quantum trajectory used for the evaluation of the action in the quantum orbits method is not unique. Due to the analyticity properties of the integrand defining the action it can be deformed as long as the integration path does not cross any singular points, which makes the location of the point where the quantum orbit intercepts the real time axis (and hence the very notion of the barrier exit time) somewhat arbitrary [11]. Furthermore, the very use of the SPM is based on the assumption that the vector potential describing the electric field is an analytic (in the sense of the theory of analytic functions of a complex variable) function of time. That need not be necessarily the case, one can easily imagine a function of time describing a perfectly realistic pulse shape which is not a complex analytic function of time. An alternative description of the tunneling ionization process must, therefore, exist, which does not make use of the complex ionization time and complex electron trajectories. We describe such a description in the present work.

In our model, introduced in [1] (see Fig. 1), an electron can tunnel and is field-ionized by a laser pulse with a peak (electric) field strength F . A direct ionization (no tunneling) happens when the field strength reaches a threshold value called atomic field strength $F_a = I_p^2/(4Z_{eff})$ [13, 14], where I_p is the ionization potential of the system (atom or molecule) and Z_{eff} is the effective nuclear charge in the single-active-electron approximation (SAEA). For $F < F_a$, ionization can happen by tunneling through a barrier which is built by an effective potential due to the Coulomb potential of the nucleus and the electric field of the laser pulse. It can be expressed in the length gauge (due to Göppert-Mayer gauge-transformation [15]) in a one-dimensional form

$$V_{eff}(x) = V(x) - xF = -\frac{Z_{eff}}{x} - xF, \quad (1)$$

compare Fig. 1. In eq 1 and hereafter, we adopt the atomic units (au), where the Planck constant, the electron's mass and charge are

* kullie@uni-kassel.de

set to unity, $\hbar = m = e = 1$. In the model the tunneling process can be described solely by the ionization potential I_p of the valence (the interacting) electron and the peak field strength F , which leads to the quantity $\delta_z = \sqrt{I_p^2 - 4Z_{eff}F}$, where F stands (throughout this work) for the peak electric field strength at maximum. In Fig. 1 (for details see [1]), the inner (entrance $x_{e,-}$) and outer (exit $x_{e,+}$) points are given by $x_{e,\pm} = (I_p \pm \delta_z)/(2F)$, the barrier width $d_B = x_{e,+} - x_{e,-} = \delta_z/F$, and the barrier height (at $x_m(F) = \sqrt{Z_{eff}/F}$) is $h_B(x_m) = I_p - V_{eff}(x_m) = \delta_z$. Which can also be obtained by two real quantities (indicating a symmetry), $h_M^\pm(x_m) = (-I_p \pm \sqrt{4Z_{eff}F})$ and we have $\|h_M\| = |h_M^+ h_M^-|^{1/2} = \delta_z \equiv \overline{h_B}$. At $F = F_a$ we have $\delta_z = 0$ ($d_B = \overline{h_B} = 0$), the barrier disappears and the direct or the barrier-suppression ionization (BSI) starts [16].

In the (low-frequency) attosecond experiments, the laser field is comparable in strength to the electric field of the atom. Usually, one uses intensities of the order of 10^{14} Wcm^{-2} .

A key quantity is the Keldysh parameter [17],

$$\gamma_K = \frac{\sqrt{2I_p}}{F} \omega_0 = \tau_K \omega_0, \quad (2)$$

where ω_0 is the central circular frequency of the laser pulse and τ_K denotes the Keldysh time.

According to Keldysh or strong field approximation (SFA), for values $\gamma_K > 1$ (actually $\gamma_K \gg 1$), the dominant process is multiphoton ionization (MPI). In the opposite case, for $\gamma_K < 1$ (actually $\gamma_K \ll 1$), a field-ionization can happen by a tunneling process, which occurs for $F < F_a$. This picture has been subsequently refined and is known now as the Keldysh-Faisal-Reiss (KFR) theory [18, 19].

As we will see, this separation between tunneling and multiphoton regime by Keldysh parameter γ_K is not rigorous, since it points to two case limits. In our model, as we will see, the classification of the two regimes (tunneling and multiphoton) is presented more clearly, when the nonadiabatic ionization (nonadiabatic field calibration of Hofmann et al. [20]) is considered. Like the adiabatic case, considered in [1], in the present work, we find that in the nonadiabatic field calibration, the field-ionization time is a time delay with respect to the quantum limit at atomic field strength F_a .

In the experiment with He-atom [2, 20], an elliptically polarized laser pulse is used with $\omega_0 = 0.061991 \text{ au}$ ($\nu \approx 735 \text{ nm}$), with ellipticity $\epsilon = 0.87$. The calibrated electric field strength is in the range $F \approx 0.02 - 0.10$ in the nonadiabatic ($F \approx 0.04 - 0.11$ in the adiabatic) case and for He-atom $I_p = 0.90357 \text{ au}$.

In the attosecond angular streaking experiment, one uses a *close-to-circular polarized laser pulse, thereby ensuring a unique relationship between the time at which the electron exits the tunnel (the potential barrier) and the direction of its momentum after the laser pulse. The measured momentum vector of the electron hence serves as the hand of a clock, indicating the time when the electron appeared from the tunnel in the laser field, see [3].* The main result of the tunneling model of Kullie [1], can be summarized with the following T-time formulas,

$$\tau_{T,d} = \frac{1}{2(I_p - \delta_z)}, \quad \tau_{T,i} = \frac{1}{2(I_p + \delta_z)}, \quad (3)$$

$$\tau_{tot} = \tau_{T,i} + \tau_{T,d} = \frac{I_p}{4Z_{eff}F}$$

The physical meaning of the relations is the following: the presence of a barrier causes a time delay $\tau_{T,d}$, which is a time delay with respect to the ionization at atomic field strength F_a , as it is defined (from the appearance intensity) by August et al. [13] (see [1] and the references therein), when the barrier disappears, $\delta_z(F_a) = 0$, $d_B(F_a) = 0$. It is the time interval during which the electron is tunnel-ionized, i.e. it ‘‘passes’’ the (emerging) barrier region (though semi-classically determined) and escapes at the exit point $x_{e,+}$ to the continuum [1]. Whereas $\tau_{T,i}$ is the time it takes to reach the entrance point $x_{e,-}$ from its initial position close to x_i , compare Fig. 1.

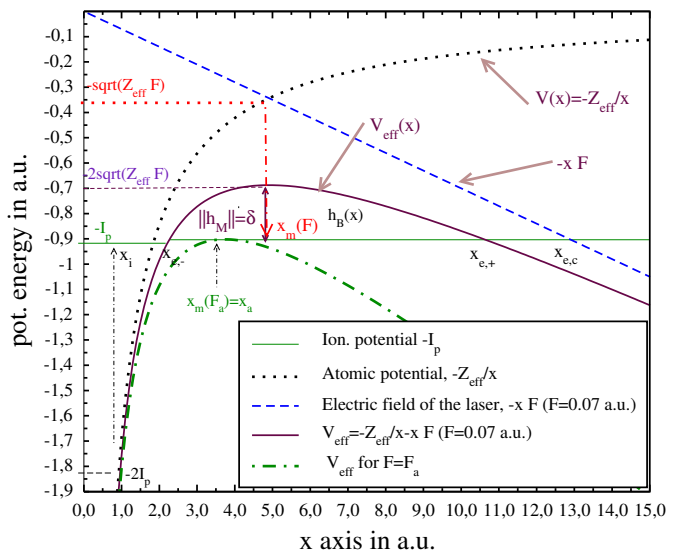


FIG. 1. (Color online) Graphic display of the potential and the effective potential curves, the two inner and outer points $x_{e,\pm} = (I_p \pm \delta_z)/2F$, $\delta_z = \sqrt{I_p^2 - 4Z_{eff}F}$, the barrier width $d_B = x_{e,+} - x_{e,-} = \delta_z/F$. I_p is the ionization potential, Z_{eff} is the effective nuclear charge and F is the electric field strength of the laser pulse at maximum. $x_{e,c} = I_p/F \equiv d_C$ is the ‘‘classical’’ exit point and $x_m(F) = \sqrt{Z_{eff}/F}$ is the position at the maximum of the barrier height $h_B(x)$, and $x_a = x_m(F = F_a)$, F_a is the atomic field strength, see text. The plot is for He-atom in the SAEA with $Z_{eff} = 1.6875$ and $I_p = 0.90357 \text{ au}$. For systems with a different Z_{eff} , I_p the overall picture stays the same.

At the limit $F \rightarrow F_a$ ($\delta_z \rightarrow 0$) the two steps coincide, the total time is $\tau_{tot} = \frac{1}{I_p}$ or $\tau_{T,d} = \tau_{T,i} = \frac{1}{2I_p}$. For $F > F_a$ we enter the BSI regime [16, 21], which is outside the scope of the present work. At the opposite limit, we have $F \rightarrow 0$, $\delta_z \rightarrow I_p$ and $\tau_{T,d} \rightarrow \infty$. Hence, nothing happens, and the electron remains undisturbed in its ground state, which shows that our model is consistent. For details, see [1, 22–24].

II. TUNNELING AND FIELD-IONIZATION TIME DELAY

In this section, we show that the time delay in our tunneling model eq 3 can be understood differently, which explains the nonadiabatic effects in principle through a multiphoton absorption, as far as the nonadiabatic field calibration is considered, as done by Hofmann et al. [20]. eq 3 can be decomposed in a twofold time delay with respect to ionization at F_a . It explains the T-time in a more advanced picture. We can rewrite the T-time $\tau_{T,d}$ in eq 3 as follows

$$\begin{aligned} \tau_{T,d} &= \frac{1}{2(I_p - \delta_z)} = \frac{1}{2} \frac{I_p}{4Z_{eff}F} \left(1 + \frac{\delta_z}{I_p}\right) \\ &= \frac{1}{2I_p} \frac{F_a}{F} \left(1 + \frac{\delta_z}{I_p}\right) \equiv \tau_a \chi(F) \\ &= \frac{1}{2I_p} \frac{F_a}{F} + \frac{1}{2I_p} \frac{F_a}{F} \frac{\delta_z}{I_p} \equiv \tau_a \zeta_F + \tau_a \Lambda_F \\ &= \tau_{dion} + \tau_{delt}, \end{aligned} \quad (4)$$

where for clarity we define the dimensionless enhancement functions $\chi(F)$, ζ_F , Λ_F for the quantum mechanical time limit τ_a . The second line in eq 4 immediately shows that our tunneling time can

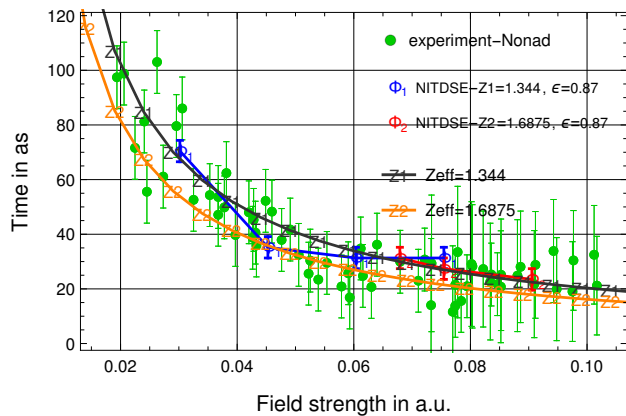


FIG. 2. (Color online) Graphic display of time delay versus field strength for He atom. The time delay $\tau_{dion}(\tau_{sym})$ as given in eq 7 (eq 8) for two Z_{eff} values, $1.344 = \sqrt{2I_p}(Z_1)$, $1.6875 (Z_2)$ [25], where I_p is the ionization potential of He-atom. Together with the experimental data of Hofmann in the new calibration of the field strength [20]. The NITDSE (see sec. A 1 and [26]: Φ_1 (blue) $Z_{eff} = 1.344$ and Φ_2 (red) $Z_{eff} = 1.6875$), with error bars of one degree (~ 4 as).

be easily interpreted as a time delay with respect to ionization time at atomic field strengths $\tau_{T,d}(F_a) = \tau_a = 1/(2I_p)$, which is real and quantum mechanically does not vanish. $\chi(F)$ is an enhancement factor for field strength $F < F_a$ (an similarly ζ_F, Λ_F). In the third line, we see that both terms are real and indicate time delays. The second term, τ_{delt} , is real because $\delta_z > 0$ is a real quantity [1]. However, as we will see, our picture corresponds to the imaginary T-time picture in the case of the adiabatic field calibration [6, 24]. In our twofold time delay picture, the first term is a field-ionization time delay solely because F is smaller than the atomic field strength F_a , whereas the second term is a time delay due to the barrier itself, which is the actual T-time as discussed in detail in the recent work [24], due to the presence of the factor ($\frac{\delta_z}{I_p}$) that specifies the (emerging) barrier height δ_z relative to the initial one I_p , in addition to the the factor (F_a/F), further below in sec. III.

We note that the separation in a twofold time delay in eq 4, represents a unified T-time picture in accordance with the Winful UTPP [27] for the quantum tunneling of a wave packet or a flux of particles scattering on a potential barrier. According to Winful [27] the group time delay or the Wigner time delay can be written in the form

$$\tau_g = \tau_{si} + \tau_{dwel}, \quad (5)$$

where τ_{dwel} is the well-known dwell time, see for example [28], which can be seen to be corresponds to our τ_{delt} , and τ_{si} is, according to Winful, a self-interference term, which corresponds to our τ_{dion} in eq 4.

From eq 4, we see that the two parts categorize two time delays with respect to the atomic field strength. An ionization τ_{dion} (with no tunneling contribution) and (an actual) tunneling τ_{delt} , where the disruption by the laser-field triggers the entire process. That is different from (but it does not contradict) the well-known premises of the strong field ionization theory, where one commonly uses γ_K to divide the process into two regimes, the multiphoton $\gamma_K \gg 1$ and the tunneling $\gamma_K \ll 1$ regime. In addition, the Keldysh time τ_K of eq 2 is rather a classical quantity, see below sec. III. The intermediate regime is assumed to incorporate a coexistence of tunneling and multiphoton ionization, and even the tunneling regime is usually extended to cover $\gamma_K \sim 1$ [2] and therefore is applied vaguely.

Fortunately, as we will see, we are able to account for the nonadiabatic effects, where a two-step model is suggested, although they

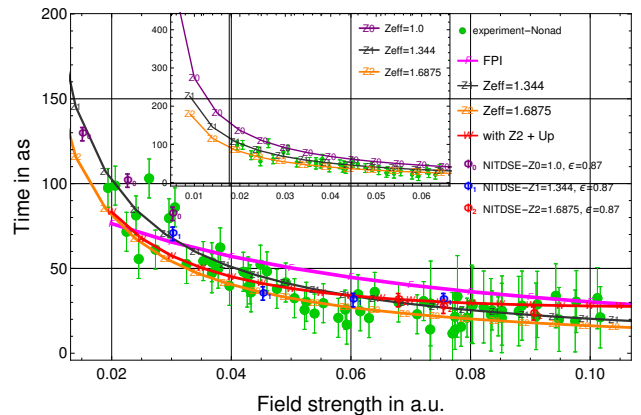


FIG. 3. (Color online) Graphic display of time delay versus field strength. Plots as given in Fig. 2 with additional curves. W-curve (red) for $Z_{eff} = 1.6875$ with $I_p \rightarrow I_p + (\frac{F}{2\omega_0})^2 \approx I_p + U_p$, where I_p is the ionization potential of He atom and U_p is the Ponderomotive potential, see [29]. The FPI result (F-curve) from [20]. An enlarged range of the axes shows that our time delay τ_{dion} gives perfectly the trend of the experimental data (see discussion in the text). In the inset the curves for three Z_{eff} (from above) 1.0, 1.344, 1.6875. The NITDSE (see sec. A 1 and [26]: Φ_0 (purple) $Z_{eff} = 1.0$, Φ_1 (Blue) $Z_{eff} = 1.344$ and Φ_2 (Red) $Z_{eff} = 1.6875$), see text.

are not strictly separated. In the first step, a scattering mechanism lowers the atomic potential barrier by the amount $\varepsilon_F = I_p - \delta_z$, whereby the energy is transferred to the electron (or electronic wave packet) by a scattering mechanism.

In the second step, traversing the barrier region (actually climbing up the remaining barrier $\delta_z = I_p - \varepsilon_F$ or the effective potential), is mainly compensated by a multiphoton absorption. Where the intermediate regime, i.e. when traversing the barrier region horizontally (horizontal channel) along with climbing the barrier (climbing the vertical energy axis, vertical channel), will be discussed in sec. V. We note that other nonadiabatic effects are small or negligible as discussed by Hofmann et al. [20]. Also, note that correlation or multielectron effects are negligible, and the SAEA is valid for He-atom, as recently shown by Majety et al. [30].

In our concept, a multiphoton absorption can be determined by the barrier height δ_z (which depends on the field strength, see Fig. 1). For now, the barrier height is largely overcome by a multiphoton absorption after the scattering with the laser wave packet (first step). We note that in the SFA such a mechanism, i.e. when multiphoton absorption accompanies the tunneling process, is usually incorporated in the intermediate regime, which we discuss in sec. V.

Our first, simplified approach follows from the physical reasoning of $\tau_{T,i}$ in eq 3. As already mentioned, $\tau_{T,i}$ is the time to reach the barrier entrance $x_{e,-}$, in the adiabatic case, where the electron encounters the barrier. It can then climb the barrier by multiphoton absorption, it reaches the top (slightly below the top) of the barrier and escapes the effective potential at x_m , compare Fig. 1. Consequently, the term due to the barrier itself is reduced by the same amount of energy. The number of absorbed (real) photons is then determined by the barrier height which can approximated by $m_F = \text{floor}(\frac{\delta_z}{\omega_0})$, where ω_0 is the central frequency of the laser pulse; the function $\text{floor}(x)$ gives the greatest integer less than or equal to x . we use the floor function instead of the ceil , since the tiny remainder ($=\delta_z - m_F\omega_0 < \omega_0$) of the potential barrier can quietly overcome by (adiabatic) tunneling, we came back to this in sec. V.

As the barrier energy reduces by the number of the absorbed

photons, that is by an amount $m_F \omega_0$, $\tau_{T,i}$ reduces as follows,

$$\begin{aligned} \tau_{T,i}(F) \rightarrow \tau_{dion} &= \frac{1}{2} \frac{I_p - (\delta_z - m_F \omega_0)}{4Z_{eff} F} \approx \frac{1}{2} \frac{I_p}{4Z_{eff} F} \\ &= \frac{1}{2I_p} \frac{F_a}{F} = \frac{1}{2I_p} \zeta_F = \tau_a \zeta_F \end{aligned} \quad (6)$$

Before we discuss the τ_{dion} , we first continue with our analysis of the nonadiabatic tunneling process, which is certainly much more complicated and richer with details than such a simple reasoning [23].

We can follow another point of view that is consistent with the commonly applied SFA to calculate the T-time. As we shall see, the adiabatic and nonadiabatic calibrations differ only by the τ_{delt} (see eq 4). It turns out that the contribution τ_{delt} (the second term in eq 4) is just due to the barrier itself, and is eliminated by the nonadiabatic calibration. This is also in line with the velocity gauge, where a barrier does not exist, which is important (compare Ni et al. [31]) and it is in accordance with the restored equivalence of the two gauges in SFA [32–34].

For the moment we assume that in the second step (after scattering in the first step), that the multiphoton absorption amounts to overcome the barrier and eliminate the second term in eq 4. We note that in their work Klaiber et al. [35] followed a similar reasoning, where the tunneling or the field-ionization can be explained in a first step by a scattering process, in which the atom is polarized by virtual multiphoton absorption, or the wave function swells and the electron scatters and gains some energy, which we can assume it corresponds to our $\varepsilon_F = I_p - \delta_z$ (first step of our view). The second step by Klaiber et al. [35] is the tunneling step from a virtual state $-I_p + n \omega_0$. The difference to the view of Klaiber et al. is that we have $\nu_F = \text{floor}(\delta_z/\omega_0) (= m_F)$ instead of an (unspecified) n by Klaiber et al. and the multiphoton absorption to be similar. eq 4 becomes τ_{dion} because the second term τ_{delt} in eq 4 vanishes, as follows

$$\begin{aligned} \tau_{dion}(F) &= \frac{1}{2I_p} \frac{F_a}{F} + \left(\frac{1}{2I_p} \frac{F_a}{F} \frac{(\delta_z - \nu_F \omega_0)}{I_p} \approx 0 \right) \\ &= \frac{1}{2I_p} \frac{F_a}{F} = \frac{1}{2I_p} \zeta_F = \tau_a \zeta_F, \end{aligned} \quad (7)$$

which is the same result of eq 6, where $0 \leq \nu_F = \text{floor}\left(\frac{\delta_z}{\omega_0}\right) \leq n_I = \text{floor}\left(\frac{I_p}{\omega_0}\right)$.

The presence of I_p is inherent to energy conservation. It implies two steps, although not strictly separated, where an energy transfer from the laser pulse to the electron by an amount ε_F by scattering (first step), or lowering the effective potential below I_p by the amount ε_F . And a second step, in which multiphoton absorption occurs to overcome the barrier (the remained effective potential) $\delta_z = I_p - \varepsilon_F$, but unlike eq 6 virtual photons absorption in eq 7 is, in principle, not excluded in addition to the real photon absorption (furthermore in sec. V), hence the notation ν_F instead of m_F , although for the moment ν_F represent a real photons number ($\nu_F \equiv m_F$).

Because $\tau_{T,i}$, $\tau_{T,d}$ leads to the same result (τ_{dion}), it becomes clear that the field-ionization time delay is a real quantity and the nonadiabatic field ionization follows directly from our adiabatic model eq 3, where only the energy conservation is required. If we consider both equations 6, 7 and realize that according to the adiabatic case, they correspond to forwards, backwards tunneling, the delay time is then the mean value (symmetrization) and we obtain,

$$\begin{aligned} \tau_{dion}(F) = \tau_{sym} &\equiv \frac{1}{2} (\tau_{T,i} + \tau_{T,d}) = \\ &= \frac{1}{2} \tau_{total} = \frac{1}{2I_p} \frac{F_a}{F} \end{aligned} \quad (8)$$

The factor $\frac{1}{2}$ is the symmetrization factor introduced in our previous work [24] to get the time delay from the Aharonov-Bohm

(ABTP) and Fujiwara-Kobe (FKTO) time operators, compare sec. 3 in [24]. Note symmetrization means an observable, i.e. physically a real quantity, which presented by a Hermitian operator (such as ABTP or FKTO, which are discussed in [24], see also [36] and the references therein, and the time-of-arrival (TOA) distribution of Simbillo et al. [37], see discussion further below), although it is still a controversial issue. The result of eq 7, 8 is fundamental and is supported by the good agreement of τ_{dion} (or τ_{sym}) with the experimental result (despite the error bars) of Hofmann et al. [20] as shown in Figs 2, 3 that we will discuss below, but let us discuss eqs 6-8 further first.

The contribution of the time delay τ_{delt} in eq 8 is removed because δ_z cancels by the symmetrization, see details in [24]. Under these considerations, it becomes unclear whether τ_{delt} is eliminated by real or virtual multiphoton absorption. However, eqs 6-8 tell us that the energy transfer can happen by either way. Therefore, we suggest that the energy gap of the neutral system (the ionization potential) can be decomposed in the form $I_p = \nu_F \omega_0 + n_F \omega_0$, where ν_F , n_F are effective numbers of virtual and real photons, they are related to the above-mentioned energy decomposition ε_F , $(I_p - \varepsilon_F) = \delta_z$, respectively. Thus, we can assume that virtual photon absorption is equivalent to a kinetic energy part (a scattering process or the polarization step in the work of Klaiber et al. [35]), whereas climbing the potential barrier is equivalent to real multiphoton absorption. We can specify the energy proportions by $\varepsilon_F \approx \nu_F \omega_0$ (scattering) and $(I_p - \varepsilon_F) = \delta_z \approx n_F \omega_0 = \nu_F \omega_0 = m_F \omega_0$ (multiphoton absorption), apart from the ponderomotive energy or the Stark-shift, see below. Still ν_F can include real and multiphoton parts, but it is unnecessary to take this into account for the moment, i.e. we put $\nu_F = m_F = \text{floor}(\delta_z/\omega_0)$.

It is straightforward to examine the limits of this energy partition. For $\lim_{F \rightarrow F_a}$ the barrier height disappears $\delta_z \approx 0$ and $n_F = 0$, $\varepsilon_F = \nu_F \omega_0 \approx I_p$, the kinetic energy transferred to the electron from the pulse (suppressing the barrier) approximately equals I_p . On the opposite side, for a small field strength ($\lim_{F \rightarrow 0}$) we have $\delta \approx I_p$, $\varepsilon_F \approx 0$ and the $I_p \approx n_{(F \rightarrow 0)} \omega_0 = n_I \omega_0$ and the barrier is overcome by real multiphoton absorption, which is equivalent to the well-know multiphoton regime of the SFA for $\gamma_K \gg 1$. Therefore, we conclude that in the range $F \sim 0.02 - 0.1$ of field strengths used by the experiment of Hofmann et al. [20], both mechanisms are present, i.e. scattering and multiphoton absorption. We are aware that the process is complicated and different effects are involved in the process. Especially, a nonlinear Compton scattering mechanism is involved [23], [38]. However, this is not critical since, firstly, their contribution is small, and secondly, they correspond to a small kinetic energy contribution, see the discussion further in sec. III, VI. Furthermore, a small (or tiny) tunneling contribution just below the top barrier related to τ_{delt} is also possible as already mentioned, which we will discuss in sec. V.

We now come to the comparison with the experimental result. The relation in eqs 7, 8 (and 6) shows a very good agreement with the experimental data in the nonadiabatic calibration of Hofmann et al. [20] as shown in Figs 2, 3, where we plot $\tau_{dion}(F)$, $\tau_{sym}(F)$ for two values of Z_{eff} , together with the experimental data of Hofmann et al. In the Fig. 2 the lowest curve (orange) for an effective nuclear charge $Z_{eff} = 1.6875$ of Clementi [25], and an upper (gray) curve for $Z_{eff} = 1.344 = \sqrt{2I_p}$ [39], where I_p the ionization potential of He-atom. As seen, the difference between the two curves is smaller than the error bars, thus, the value of Z_{eff} is not crucial. In Fig. 3, we also plotted $\tau_{dion}(F)$ for $Z_{eff} = 1.0$ (inset, purple) and a curve for $Z_{eff} = 1.6875$ (red, W-curve) by including the energy (continuum) shift given by $(\frac{F}{2\omega_0})^2$ [29] (chap. 2, p.19), i.e. by replacing I_p with $I_p + (\frac{F}{2\omega_0})^2$ ($\approx I_p + U_p$, where U_p the Ponderomotive potential), which is negligible for $F < 0.05$. We also included in Fig. 3 the Feynman path integral (FPI), (magenta, F-curve), from the same work of Hofmann et al. [20].

Furthermore, we show in the figures our calculated result of the NITDSE, see sec. A 1 and [26], for $Z_{eff} = 1.6875, 1.344$ in Fig. 2

and also for $Z_{eff} = 1.0$ in Fig. 3. As seen in the figures, NITDSE is in an excellent agreement with our τ_{dion} result and confirms our model.

Looking back to the NITDSE result of Ref. [26], one finds that the NITDSE was compared to experimental data of Boge et al. [40] using a nonadiabatic calibration, see further below sec. VI. The data of Boge et al. [40] (below Fig. 7) differs slightly (a bit higher) from the data of Hofmann et al. [20], so that the NITDSE result of Ivanov et al. [26] was not close to the experimental data of Boge et al. as it is the case in Fig. 2, 3, see also the discussion in [23]. Finally, the good agreement between these results, our result, the NITDSE, and the recent experimental data of Hofmann et al., shows that our point of view offers a reasonable explanation of the issue.

Most likely $Z_{eff} = 1.0$ fits better for small field strengths, although no experimental result is available, compare Fig. 3 (inset, upper curve). The fact that $Z_{eff} = 1.0, 1.344$ becomes closer to the curves of $Z_{eff} = 1.6875$ towards F_a region is because Z_{eff} has a lower weight in the product ($Z_{eff}F$) for larger F values, but one can easily see that the slope of $Z_{eff} = 1.0$ curve does not match to the experimental values in the region $F = 0.2 - 0.5$. Also note that despite the importance of the FPI result [2] (see [28], [1]), it does not fit well with the experimental data, in particular the trend is not satisfactory. In contrast to the flat behavior for larger field strengths, for smaller field strengths $F \leq 0.02$ the T-time becomes very steep with a large slope, see Fig. 3. One might even think that the (ionization) time delay τ_{dion} (τ_{sym}) of eq 7 (eq 8) is valid for small field strengths.

The good agreement of our result with the experimental data as shown in figs 2, 3 indicates that the main behavior of the time delay is determined by the $\sim \frac{1}{F}$ dependence, which is similar to the classical behavior or the Keldysh time eq 2 [22]. One also notices that both scale similarly with the ionization potential, Keldysh time $\tau_K \sim \sqrt{2I_p}$ and our time delay $\tau_{dion} \sim \frac{I_p}{Z_{eff}} \sim \sqrt{2I_p}$. Apparently, τ_K is a classical quantity, while our time delay is the corresponding quantum mechanical quantity.

Note on one-Dimensional model

Finally, we note that the agreement of our one-dimensional (1D) model with the three dimensional (3D) NITDSE is not surprising. The 1D model (along with the 3D model) is widely used in the attoclock and attosecond science [41–48]. It is justified by the well known fact that (tunnel-) ionization in strong field regime occurs primarily along the direction of the electric-field at maximum, see [41, 48]. Then, the tunneling probability increases with decreasing width of the barrier ($\sim \frac{1}{F}$ dependence, $d_B = \delta_z/F$ see Fig. 1); and the most probable tunneling path is concentrated along the electric-field direction at maximum. The longitudinal contribution of the Coulomb potential into the dynamics represents the leading-order, while the transversal effect of the Coulomb potential is a higher-order correction [41, 48].

In fact, the attoclock scheme [3, 4, 49] enables one to indicate the departure of the 1D model from the 3D-model, where the 1D-axis is along the barrier width. For a circular polarized laser pulse, the (tunnel-) ionization occurs primarily along the direction of the electric-field at maximum every half cycle, giving rise to a twofold symmetry of the electron momentum distribution in the polarization plane. The deviation of the orientation of the twofold symmetric distribution is referred to as angular offset [49]. Thus, for a close to circular polarized laser pulse, the deviation from the twofold symmetric distribution depicts the deviation from the 1D-model (tunnel-) ionization along the barrier width. Therefore, the asymmetry shown in Fig 8, which characterizes the orientation of the electric-field in the period of (tunnel-) ionization time (the angular offset), implies the small deviation of the 1D-model (along the barrier width) from the 3D-model.

With this and similar to the note in [41], we give an estimate

of the deviation of the 1D-model from 3D-model. As seen in Fig 8 (sec. A 1), $\frac{p_x}{p_y} \sim (0.25/1.5) \sim 17\%$ (the propagation direction is along the z-axis). The minimum of the barrier width is reached at the atomic field strength F_a . In our case, we have $F_a \sim 0.12 au$, which is the values used in the figure Fig 8. Accordingly, the deviation perpendicular (xy - or ellipticity-plane) to the 1D-along-barrier (z -axis) is expected to be of a second order of the barrier width at $F \sim 0.12 au$, and we could assume a similar percentage for lower field strengths. Now, keeping in mind that the distance along the path (curve) covered by the (tunnel-) ionized electron can be approximated by the simple arithmetic relation

$$d_{path} \approx \sqrt{d_{\parallel}^2 + d_{\perp}^2} = \sqrt{d_{\parallel}^2 + ((0.25/1.5) * d_{\parallel})^2} \sim 1.02 d_{\parallel},$$

where d_{\parallel} (d_{\perp}) is the 1D-distance along (perpendicular to) the barrier width, see Fig 1. As we see, the effect is only about $\Delta d_{path} \sim 2\%$ for $F = 0.12 au$. Since the deflection angle is small, we can also use the arc ($s_{\phi}(F)$) (as calculated by NITDSE) and get for $Z_{eff} = 1.6875$, $\Delta d_{path}(s_{\phi}) \leq 5\% d_{\parallel}$ (or $\lesssim 15\% d_{\parallel}$ for $Z_{eff} = 1.0$) in the range of the applied field strengths. Thus, we expect that the effect on the time delay is of the same order $\sim 5\% - 15\%$ for $Z_{eff} = 1.6875 - 1.0$, respectively. It is a second-order correction, much like the claim of [41] mentioned above. The effect on the time duration for $Z_{eff} = 1.6875$ is $\sim 5\% \cdot \tau_d \approx 1 - 5 as$ (or $\lesssim 3.5 - 20 as$ for $Z_{eff} = 1.0$) in the range $F = 0.1 - 0.02$, respectively. It is about or less than the error bars given by the experiment and the error bars given by the NITDSE calculation of one degree (offset angle) $\sim 4 as$ in the Figs 2, 3. It is worth noting that in strong field regime, the correlation do not have a significant effect on the offset angle [30]. To conclude, the 1D-model is justified in strong field regime and only for small field strengths less (or much less) than $0.01 au$, the discrepancy between 3D- and 1D-model of the streaking angle is significant.

III. DISCUSSION

Looking to $\tau_{dion} = \tau_{sym} = \frac{1}{2} \frac{I_p}{4Z_{eff}F}$ we see that I_p determines the ionization time, although the barrier height is δ_z , compare Fig. 1. When the laser pulse (wave packet) scatters on the atom and its field F bends the atomic potential curve, the gain of the energy ε_F corresponds to the strength of the bending or lowering the barrier below the continuum (first step), compare Fig. 1. Since, in such a case, it is usual to use the concept of virtual photon, we write ε_F in the form $\varepsilon_F \approx v_F \omega_0$, where v_F denotes the number of the virtual photons.

Thus, due to the conservation of the energy, we can write $I_p = \varepsilon_F + \delta_z$, $\delta_z \approx n_F \omega_0 (= v_F \omega_0 = m_F \omega_0)$ (apart from a tiny remainder as already mentioned and the Ponderomotive energy or the continuum Stark-shift [29] p. 19, compare Fig. 3 W-curve), where for the sake of simplicity we use the notation n_F . n_F ($0 \leq n_F = \text{floor}(\delta_z/\omega_0) \leq n_I$) is the (minimum) number of photons required to (climb) overcome the barrier height (second step) at a field strength F , which is the barrier or energy gap δ_z for the interacting electron [22], compare Fig. 1. Therefore, the presence of I_p in τ_{dion} indicates that both steps take (real) time to happen, as it should be.

It is worthwhile to mention that our real time (delay) picture is consistent with the approach discussed by Klaiber et al. [35, 50] (furthermore in sec. VI), whereas in the imaginary T-time picture or instantaneous tunneling, see e.g. [5, 51], the offset angle measured by the experiment is attributed to the tail of the potential. The first term ε_F is implicitly considered, as the first step (e.g. by Sainadh et al. [5]) and claimed to be the collapse of the wave function in the orthodox interpretations of the QM and to be in zeptosecond range [5]. A similar conclusion is claimed by Ni et al. [31, 52] using classical back propagation. One finds that the aforementioned imaginary T-time picture approach (instantaneous tunneling) agrees with the adiabatic field calibration, which can

be compared with our adiabatic T-time picture $\tau_{T,d}$ (eq 3), which agrees well with the experimental result for H-atom [5] and the accompanied NITDSE result as discussed in [6], apart from a factor $1/2$, which is discussed in [24].

In the perturbation regime where F is small, we have $\delta_z \approx I_p$, $n_F = n_I$, whereas for a strong field one easily finds that the number of absorbed photons is decreased by a factor that depends on the field strength $0 \leq n_F \approx n_I \sqrt{1 - F/F_a}$. In other words, n_F is the threshold number of photon required to satisfy the energy conservation with $I_p = \varepsilon_F + \delta_z$ ($\varepsilon_F \approx (n_I - n_F)\omega_0$), which, i.e. n_F , is not taken into account in the adiabatic tunnel-ionization (relative to I_p of the perturbation regime.) Then, $\varepsilon_F = I_p - \delta_z \equiv \Delta E$ can be used as an energy uncertainty and by the virtue of the uncertainty principle, we have $\tau_{T,d} = 1/(2\Delta E) = 1/(2(I_p - \delta_z))$, as given in eq 3, see [1, 5, 6, 22] for details. For $F \rightarrow F_a$ we have $\varepsilon_F (\equiv \Delta E) \rightarrow I_p$, $n_F = 0$, the barrier $\delta_z(F = F_a) = 0$ vanishes and the delay time reaches its quantum limit $\tau_{T,d} = \tau_{dion} = 1/(2I_p)$, as already discussed. At the opposite limit $F \rightarrow 0$, $n_F = n_I$, $v_F \rightarrow 0$, $\varepsilon_F \rightarrow 0$, $\delta_z(F = 0) = I_p$. In this case we have $\tau_{T,d} \rightarrow \infty$, $\tau_{dion} \rightarrow \infty$ and the electron stays undisturbed in its ground state. Further below in sec. V.

It is worthwhile to mention that our model is consistent with the result of Sombillo et al. [37] for the time distribution of an incident particle using the TOA formalism. In fact, Sombillo et al. concern in their work the TOA operator and suggest an interpretation of TEUR, which is in line with our point of view. They found that as the width increases, the traversal peak time moves to higher values like our time delays, whereas in the opposite direction, it results in a traversal-time distribution with a peak shifted towards lower values of time, that is in our model when $\tau_{T,d}$ reaches the quantum limits $1/(2I_p)$ at $F = F_a$, which explains the Hartman effect.

With our model of eqs 3–8 we found a correspondence between the time delay of adiabatic and the nonadiabatic field-ionization, which agree well with the experimental results in both cases of the field calibrations, the nonadiabatic and adiabatic, for He atom [20] and [2] (and [5] for H-atom), respectively.

At this point, looking to eq 4 (second line), it seems that in the nonadiabatic calibration the time delay is determined by τ_{dion} in the sense that the nonadiabatic effects beyond multiphoton absorption are small, whereas the adiabatic calibration is identified by the presence of a second term, the barrier term δ/I_p , which give τ_{delt} . Then, the enhancement factor $\zeta_F = F_a/F$ is present in both cases and manifests the time delay $\tau_{dion} = \tau_a \zeta_F$, which is the (ionization) time delay in the nonadiabatic calibration, precisely assuming that other nonadiabatic effects beyond the multiphoton absorption are negligible. It corresponds to the self-interference term introduced by Winful (eq 5) in the UTTP.

Considering the experimental data of Hofmann et al. [20] to present the correct calibration (apart from the error bars) to the tunneling issue (or to the field-ionization and field calibration in strong field region), we think that our explanation provides a clear and comprehensive picture for the field-ionization (or tunnel-ionization) in the strong field and the attoclock. It enables us to describe very well both experimentally constructed results for He- and H-atom, the adiabatic in [1], [6] and the nonadiabatic in the present work for He-atom. Interestingly, our result shows an excellent agreement with the NITDSE result as seen in figs 2, 3. The agreement with the NITDSE greatly supports our model. Note that in eqs 4-8 the enhancement factors ζ_F , Λ_F , χ_F are relative dimensionless factors, and we can use the intensity instead of the field strength, $F/F_a = \sqrt{I_L/I_a}$, where I_a is the appearance intensity [13] and I_L the intensity of the laser pulse.

From the result in eqs 7-8 and figs 2-3 and our discussion so far, we conclude that the interaction with the strong field can also be understood as a combined process of a scattering (ε_F) and a multiphoton absorption ($n_F\omega_0$), as far as nonadiabatic calibration is concerned, e.g. as done by Hofmann et al. [20], where other nonadiabatic effects are small or negligible, as already mentioned, which implies that energy gain beyond multiphoton absorption can be neglected. The question is what or where is the difference be-

tween the weak and strong field interaction processes, by neglecting the (smaller) nonadiabatic effects beyond the multiphoton absorption (e.g. pulse duration or change of field strength during the period of traversing the barrier region or intensity fluctuations). In fact, these effects are noticeably below the error bars. Obviously, a main effect is the scattering process and polarization of the electronic wave packet [35], [23], or the shrinking of the (energy) gap I_p down, it becomes $\delta_z(F) < I_p$ up to $\delta_z \approx 0$ at $F = F_a$, whereas for small field strength $\delta_z(F \rightarrow 0) \approx I_p$.

The time delay decreases with increasing field strength F (and vice versa), in accordance with the uncertainty principle [7, 22, 37], and is determined by the enhancement factor ζ_F (or $\chi(F)$ for the adiabatic case), which becomes unity at $F = F_a$, at which the ionization time reaches its lower quantum limit $\tau_{dion}(F_a) = \tau_a = 1/(2I_p)$. Nevertheless, as far as nonadiabatic effects are concerned, we can imagine that the above-mentioned two steps happen simultaneously. Similarly, many authors, e.g. Ivanov et al. [32] and Klaiber et al. [35], [50], maintain the point of view that the energy gain can be thought as of an absorption of photons during the tunneling process. In [50] the authors claim that in the nonadiabatic regime the energy gain (including a multiphoton absorption) occurs during the course of the under-the-barrier motion, where they describe the nonadiabatic energy gain semi-classically (with a classical action) [35, 50] see below Fig. 7, we come back to this point later in sec. V, VI.

The error bars of the experiment are large (see Fig. 2, 3), which makes it harder to verify that after photons absorption, tunneling occurs slightly below the top of the barrier. Indeed, one can better understand this point by eliminating the other nonadiabatic effects, e.g. due to laser pulse duration (envelope), rotating of the laser field during the period of field-ionization and intensity fluctuations, which can be responsible for the spread of experimental points, see sec. V. Hofmann et al. [53] noted that between recording one distribution to the next, the laser parameters, setup, temperature in the lab, ... might change and have a slight influence, in principle the data point should also have error bars for their F-axis-position. By the multiphoton absorption $\sim n_F$, a tunneling mechanism can happen just below the threshold, or slightly below the top of the barrier as already mentioned, where $\frac{\delta_z}{\omega_0}$ is usually not an integer, and the absorption of n_F photons lets a fairly small energy gap $\frac{\delta E}{\omega_0} = (\frac{\delta_z}{\omega_0} - n_F) < 1$, which permits a tunneling mechanism, we will discuss this further in sec. V. The interaction process is more complicated and a complex scattering mechanism and a nonlinear Compton scattering can be involved, where energy and momentum are transferred to the tunneled or ionized electron by the scattering process, see [23]. They are related to the characteristic of the interaction of the electron with the intense laser field [54] by $\sim \left(\frac{F}{\omega_0}\right)^2$ and $\sim \alpha \left(\frac{F}{\omega_0}\right)^2$, respectively. $\alpha = 1/c$ (c the speed of light in vacuum) is the fine structure constant, which is equal to the strength of the interaction of the photon with the electron. We are aware that our result in eqs 6-8 and 3, 4 should be understood as a well-estimated result for the time delay, which could serve as a step for an extension towards more sophisticated quantum mechanical treatment.

It is worthwhile to mention that many authors use a different definition for the atomic field strength, e.g. $F_a^K = k^3 = (2I_p)^{3/2}$ [10, 50], which is related to the Keldysh parameter. It leads to the Keldysh time as we can see by the substitution $F_a \rightarrow F_a^K$ in eqs 7, 8,

$$\frac{1}{2I_p} \frac{F_a^K}{F} = \frac{1}{2I_p} \frac{k^3}{F} = \frac{2I_p \sqrt{2I_p}}{2I_p F} = \frac{\sqrt{2I_p}}{F} = \tau_K$$

It is well known that Keldysh time is too large, a classical quantity and does not describe tunneling or field-ionization time (delay), for details see [22]. This, however, shows that our time delay τ_{dion}, τ_{sym} (eqs 6-8) is directly connected to SFA, where F_a (thus δ_z [1]) represents the correct parameter to determine the time delay while the atomic field strength is given by $F_a = I_p^2/4Z_{eff}$ [1, 13, 14] regardless of the Keldysh parameter γ_K . Considering

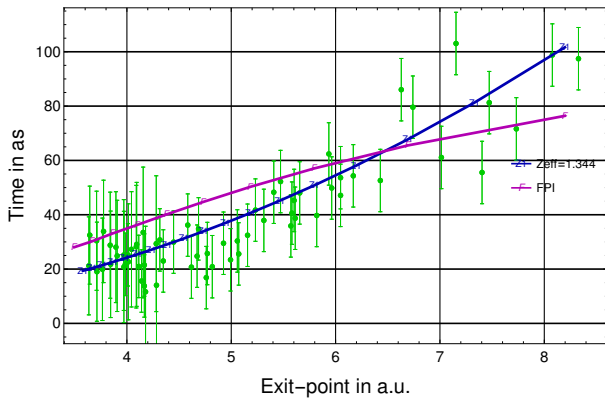


FIG. 4. (Color online) Graphic display data of Hofmann in the new calibration of the field strength, with our time delay τ_{dion} versus exit point $x_m = \sqrt{Z_{eff}/F}$, with $Z_{eff} = 1.344$ (a similar behavior is found for $Z_{eff} = 1.6875$). F-curves denote FPI-curve.

the field strengths given by the experimental results, the Keldysh parameter is in the range of $\gamma_K \approx 0.76 - 2.2$ in the adiabatic [2] and in the range $\gamma_K \approx 0.8 - 4.3$ in the nonadiabatic case [20]. Hence, despite its importance for the SFA, the Keldysh parameter loses its significance in this regime, commonly referred to as the intermediate regime, see sec. V.

In summary, in the strong field regime the nonadiabatic field calibration can be understood by a scattering process combined with a second step, which is essentially a multiphoton absorption. The number of absorbed photons can be approximated by n_F , $0 \leq n_F = \text{floor}(\frac{\delta_z}{\omega_0}) \leq n_I \omega_0$. The scattering process can be understood in a semiclassical sense that the (electric) field of laser pulse bends the (atomic) potential barrier, which reduces the energy gap from I_p to δ_z , apart from the (continuum) Stark-shift [29] and neglecting the small contribution of other nonadiabatic effects, see sec. V. This picture is well-supported by the good agreement of our τ_{dion} , τ_{sym} (eqs 6-8) with the experimental results as shown in figs 2, 3 in the nonadiabatic case of Hofmann et al. [20]. And in the adiabatic case (eqs 3, 4) of Landsman et al. [2], as previously shown in [1] for He-atom and in [6] for H-atom. Our result is strongly supported by the NITDSE. For small F the gap becomes close to the ionization potential $\lim_{F \rightarrow 0} \delta_z = I_p$ and $n_F = n_I$. In the perturbation regime, i.e. a low-intensity (a relatively small field strength) and a low-frequency ($\text{floor}(I_p/\omega_0) \gg 1$), a (non-resonant) ionization happens by multiphoton absorption of $\sim n_I$ photons (usually $n_I + 1$ is used, or the *ceil* instead of *floor* function [29]). We think that eqs 7, 8 can be also valid in this case or serve as a good approximation, as we can see from Fig. 3. Finally, our model in the nonadiabatic case is related to the adiabatic case and although it follows a simplified approach, it is important because it enables us to provide a detailed (but not sophisticated) picture of the strong field interaction with the laser pulse, in accordance with the Winful UTP, which is important for the tunneling theory in general. Indeed, this is one of the reasons why it makes sense to study the adiabatic and nonadiabatic field-ionization together, as there exist two field calibrations for the same experiment and system (He-atom).

IV. THE EXIT POINT

It is common in the strong field and ultra-fast science to use the so-called classical exit point $x_C = I_p/F$, see Fig. 1, to characterize the spatial location of the point at which the tunneled or ionized electron escapes the potential barrier or the effective potential, for details see [22]. Depending on the concept used to characterize the tunneling process, it becomes free when it exits the “exit” point (‘real’ T-time picture [1]), or it becomes subject to the tail of the potential (imaginary T-time picture [5]). A quick look at Fig. 1

shows immediately that $x_C = I_p/F \equiv d_C$ is inaccurate and even wrong. For the adiabatic tunneling, it was shown in [55] that (in a semi-classical picture) the correct exit point is $x_{e,+}$ (compare Fig. 1) and the use of x_C (or d_C) leads to an erroneous conclusion. In our nonadiabatic model (the present work), the exit point $x_{e,+}$ is not suitable because multiphoton absorption is now involved, apart from other nonadiabatic effects. Thus, we expect a major effect on the exit point. At first glance, this effect might result in an exit point equal to $(1/2)x_C$ (eq 9 below), but as we will see, this may not be the correct approach and another approach is presented below.

Recalling what we did in eqs 6, 7 we find:

$$x_E = \frac{I_p \pm \overbrace{(\delta_z - n_F \omega_0)}^{\approx 0}}{2F} = \frac{I_p}{2F} = \frac{1}{2} x_C, \quad (9)$$

where the initial point is close to $x_i \sim 1au$ (see fig 1), it is small and can be fairly neglected. We note that with eq 9 the barrier width vanishes $d_B = x_{e,+} - x_{e,-} = 0$, whereas the traversed distance in this case is $d_h = x_{exit} - x_{initial} \approx x_E$. Nevertheless, because $x_E = x_C/2$ the overall picture is similar to the case of the adiabatic calibration, see Fig. 2 of [55]. This shows a linear dependence of the time delay versus the exit point (the same $\sim \frac{1}{F}$ dependence of eqs 7, 9), which is most likely unsuitable for such a process.

The multiphoton absorption is usually depicted as a vertical channel [32], i.e. the electron climbs the effective potential and moves towards its maximum. Hence, we can characterize the exit point in this way. As seen in Fig. 1, the maximum of the barrier height is located at $x_m = \sqrt{Z_{eff}/F}$ and we expect that the ionized electron, climbing the barrier, will move towards x_m . In Fig. 4, we plot the ionization time τ_{dion} versus the exit point for the two $Z_{eff} = 1.344, 1.6875$. Unlike x_E , the exit point x_m , and hence, the curves in Fig. 4 depend on Z_{eff} . The difference to the former case (linear dependence) is not remarkable, although x_m is noticeably smaller. In addition, it is difficult to judge from Fig. 4 whether x_m actually determines the exit point. Nevertheless, from the good agreement of τ_{dion}, τ_{sym} with the experimental data (as seen in Fig. 2) for Z_{eff} values larger than 1.0, i.e. $Z_{eff} = 1.6875, 1.344$, we think that the traversed distance by the ionized electron should not be too large (not too far from the nucleus.) Since x_m is smaller than x_E (eq 9), the actual exit point is most likely close to x_m , see further below sec. V. This is unlike the adiabatic case, where no photon absorption is involved in the tunneling process. In the later case, the horizontal channel dominates the process of tunneling (tunnel-ionization) [32]. Finally, the so-called classical exit point x_C is by no mean a correct choice (compare Fig. 1), see also [55] for the adiabatic case. Indeed, it is easy to see from the barrier width, $d_B = \frac{\delta_z}{F} = \frac{I_p}{F} \sqrt{1 - 4Z_{eff}F/I_p^2} = x_C \sqrt{1 - F/F_a}$ that x_C is modified by a factor that becomes approximately unity for small field strength, $\lim_{F \rightarrow 0} \sqrt{1 - F/F_a} \rightarrow 1$. Hence, the so-called classical barrier width is justified only for $F \ll F_a$ ($\gamma_K \gg 1$). To conclude, it is difficult to determine the “correct” exit point with our approach. In the nonadiabatic case, one finds that the exit point of the field-ionized electron is close to $x_m = \sqrt{Z_{eff}/F}$, but $x_E = I_p/(2F) = (1/2)x_C$ is also not excluded. In any case, it is in a range between x_m and x_E , see further below, and not $x_C = I_p/F$ as usually done, e.g. [20].

V. THE INTERMEDIATE REGIME

In our model we have treated so far two experimentally given cases, the nonadiabatic field calibration for He-atom in the present work and the adiabatic field calibration case for He atom in [1] and for H-atom in [6]. In both cases, we found a good agreement with the experimental result. The field calibration of Hofmann et al. [20] affects a shift to a lower intensity. It causes a shift of the time delay to a smaller value for the same field strength. This confirms our tunneling model as seen in eq 4,7, since the second term vanishes $\tau_{delt} = 0$, when both a scattering and multiphoton

absorption process are involved. A feature of the experimental data (both adiabatic and nonadiabatic, see below Fig. 6) is the spread of the points. This can be for a variety of reasons, such as pulse length or carrier envelope phase. However, as we will see below, this can also be caused by intensity fluctuations that allow a tunneling contribution slightly below the top of the barrier.

The two cases of the field calibration can also be viewed as two limits to the field-ionization process. This immediately raises the question about what is usually called the intermediate regime, in which both a tunneling contribution and a multiphoton absorption exist [32].

In deriving τ_{dion} (τ_{sym}) we assumed that the number of absorbed photon and the gain of the energy due to the scattering with the laser wave packet, preserves the energy conservation $I_p \approx \varepsilon_F + n_F \omega_0$ (approximately as $n_F = \text{floor}(\delta_z/\omega_0)$), apart from the Stark-shift [29] or the Ponderomotive energy. Nevertheless, due to the complexity of the process the above-mentioned two steps are not strictly separated, and the electron can also escape by following a horizontal channel [32] while it climbs up the energy axis (vertical channel), and ends up with an energy $(\varepsilon_F + \varepsilon_{\omega_0}) \sim I_p$, regardless the relative number of the (virtual and real) absorbed photons. More specifically, we can write $I_p = (\varepsilon_F + \varepsilon_{\omega_0}) + \Delta\varepsilon$. For $\Delta\varepsilon \approx 0$ we have $(\varepsilon_F + \varepsilon_{\omega_0}) = \varepsilon_F + n_F \omega_0 \approx (\varepsilon_F + \delta_z) \approx I_p$ corresponds to τ_{dion}, τ_{sym} of eqs 7, 8. Note, that the absorption of photons number larger than n_F required by the energy conservation, is equivalent to an above-threshold ionization (ATI) process, similar to the well known non-resonant ionization [56] in the perturbation regime. In the following, we do not consider the ATI process, with the possibility of addressing it in a future work.

However, $(\varepsilon_F + \varepsilon_{\omega_0}) + \Delta\varepsilon > I_p$ (apart from U_P) means that the energy gain becomes larger than the maximal barrier height I_p and the electron escapes with a velocity larger than zero. Therefore, in accordance with the SFA that the momentum peaks around zero velocity, we assume that $\Delta\varepsilon$ is small. In a first approach we approximate $\Delta\varepsilon$ and set $\Delta\varepsilon \approx \Delta n \omega_0$, $\Delta n = \text{floor}(\frac{\Delta\varepsilon}{\omega_0})$, where Δn is small compared to $n_F = \text{floor}(\frac{\delta_z}{\omega_0})$. eq 7, 8 then becomes

$$\begin{aligned} \tau_{t ion}(F) &= \frac{1}{2} \frac{I_p + \Delta\varepsilon}{4Z_{eff}F} \\ &= \frac{1}{2I_p} \left[\frac{F_a}{F} \left(1 + \frac{\Delta n \omega_0}{I_p} \right) \right] \\ &= \tau_a \eta(F, \omega_0, \Delta n) \end{aligned} \quad (10)$$

In eq 10 the gain of the energy happens while the electron is non-adiabatically field-ionized by absorbing a number of photons corresponds to $n_F + \Delta n$. We mention that a similar view is presented by Camus et al. [57].

Likewise, as discussed in sec. II when we obtained eq 7, another point of view can be considered, in which the electron (or the electron wave packet) tunnels by absorbing an effective number of photons $\tilde{n}_F < n_F$ so that τ_{delt} does not vanish (compare eq 7), while the first term (self-interference term according to Winful UTTP) is preserved by the virtue of the energy conservation. In this case, we have $\varepsilon_F + \tilde{n}_F \omega_0 + \Delta\varepsilon \gtrsim I_p$, with an effective number of real photons $\tilde{n}_F \lesssim n_F$. $\Delta\varepsilon$ is small, in accordance with the SFA, where $\Delta\varepsilon$ corresponds to a tunneling contribution (horizontal channel). With $\Delta\tau_{delt} = \frac{\Delta\varepsilon}{4Z_{eff}F}$, and $\Delta\varepsilon = \Delta\nu \omega_0$ ($\Delta\nu \approx \text{floor}(\frac{\Delta\varepsilon}{\omega_0})$) and from eq 4 or eq 7, we obtain

$$\begin{aligned} \tau_{t ion}(F) &= \tau_{dion} + \Delta\tau_{delt} \\ &= \frac{1}{2I_p} \left[\frac{F_a}{F} \left(1 + \frac{\Delta\nu \omega_0}{I_p} \right) \right] \\ &= \tau_a \eta(F, \omega_0, \Delta\nu) \end{aligned} \quad (11)$$

And again $\Delta\varepsilon = 0, \Delta\nu = 0$ corresponds to eq 7 or 8. In eq 11 the energy gain happens by absorbing \tilde{n}_F photons followed by a small tunneling contribution a little below the top of the barrier. This is similar to the view of Klaiber et al. [50], more on this in sec. VI.

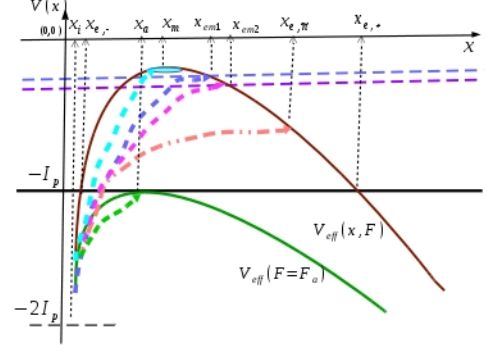


FIG. 5. (Color online) Illustration of the intermediate regime, eqs 11-13. The (orange) dashed dotted curve illustrates the view of Klaiber et al. [50], which is usually called the nonadiabatic or intermediate tunneling regime [32], see text eqs 11, 13. See also Fig. 1.

At first glance, we can imagine that an energy gain occurs during the entire process, where horizontal and vertical channels coexist [32]. However, if one imagines that such a process takes place in a complex mechanism, in which an energy gain occurs even after it tunnels/escapes the exit point, we are led to the imaginary T-time picture discussed by Sainadh et al. [5] and recently [51]. Note that for $\Delta\nu \rightarrow \nu_F$ ($\Delta\tau_{delt} \rightarrow \tau_{delt}$), eq 11 becomes identical to eq 4 (or $\tau_{T,d}$ in eq 3), which is the adiabatic case. We emphasize that our (real) T-time picture in the adiabatic case agrees well with the imaginary T-time picture for H-atom and with the NITDSE [6, 51]. This undoubtedly confirms our view.

As seen in eqs 11 (eq 10), the time delay increases for $\Delta\nu > 0$ (or $\Delta n > 0$) and becomes larger than the field-ionization time delay given by τ_{dion}, τ_{sym} (or the self-interference term τ_{si} according to eq 5 in the UTTP of Winful [27]). With eq 11 the situation now becomes similar to so-called intermediate tunneling regime, where the vertical and horizontal channels co-exist [32]. Eq 10 becomes identical with eq 11 by the replacement $\Delta\nu \rightarrow \Delta n$, where eq 11 is suitable (with $\Delta\nu$ virtual photons number) to describe a tunneling mechanism [35] and, as we will see, to explain that the time delay increases by moving from the nonadiabatic towards an adiabatic field calibration or adiabatic tunneling, which is significant for the tunneling theory. And, as we will see, it explains the spread of the experimental points, which can be caused by intensity fluctuations of the laser pulse. Therefore, we restrict our discussion to eq 11. For tiny $\Delta\varepsilon$ the tunneling through the horizontal channel happens just under the top of the barrier, as depicted in Fig. 5, where the tunneling probability is notably high.

We summarize the time delay as the following

$$\tau = \begin{cases} \tau_{dion} = \tau_a \zeta(F) & \text{eqs 7, 8, nonadiabatic} \\ \tau_{T,d} = \tau_a \chi(F) & \text{eqs 3, 4, adiabatic} \\ \tau_{t ion} = \tau_a \eta(F, \omega_0, \Delta\nu) & \text{eq 11, "intermediate"} \end{cases}$$

The summary is detailed in table I. With this, we can treat the intermediate regime, which is generally considered to be multiphoton absorption during tunneling. It was first described by Ivanov et al. [32] and the conclusion was that the two channels (horizontal and vertical) do not exclude each other. According to Ivanov they co-exist in a ‘gray’ area $\gamma_K \approx 1$, called ‘nonadiabatic tunneling’. Similarly, Klaiber et al. in [35] presented a view that can be compared with our view in the following. In our nonadiabatic picture, the horizontal channel (tunneling) is a little below the top of the barrier. In Fig. 5, we show an illustrative picture of two intermediate cases, in which the multiphoton absorption is followed by a tunneling from two intermediate virtual states below the top of the barrier (the two horizontal dashed lines in Fig.

Regime	Time delay expression	Enhancement expression
Nonadiabatic	$\tau_{dion} = \tau_{sym} = \frac{1}{2I_p} \frac{F_a}{F}$	$\tau_a \zeta(F)$
Adiabatic	$\tau_{T,d} = \frac{1}{2I_p} \frac{F_a}{F} \left(1 + \frac{\delta_z}{I_p}\right)$ $= \tau_{dion} + \tau_{delt}$	$\tau_a \chi(F)$ $= \tau_a (\zeta(F) + \xi(F))$
Intermediate	$\tau_{t ion} = \frac{1}{2I_p} \frac{F_a}{F} \left(1 + \frac{\Delta\nu \omega_0}{I_p}\right)$ $= \tau_{dion} + \Delta\tau_{delt}$	$\tau_a \eta(F, \omega_0, \Delta\nu)$

TABLE I. The table summarizing the regimes and their associated time delay expressions.

5). We illustrate this with the two dashed curves blue and purple, from above the second and third (dashed) curves under the barrier, with the exit points x_{em1}, x_{em2} (see below), respectively. Whereas the highest dashed curve (light blue, from above the first dashed one), illustrates the case of a negligible tunneling contribution (where $\delta_z - n_F \omega_0 < \omega_0$), with the exit point $\approx x_m$. A lower dashed-dotted curve (orange, from above the fourth one curve) corresponds to the view of Klaiber et al. [50], according to which the tunneling happens significantly below the top of the barrier. We will come back later to this in sec. VI.

In addition, the limit case for $F = F_a$ is shown in Fig 5, green dashed curve (the lowest curve with the exit point $x_m(F_a) = x_a$). In this case, the atom is highly polarized that the barrier disappears and the BSI sets up. The time to reach the entrance point x_a (which coincides with the exit point) is the quantum limit τ_a , see eqs 7, 8. This picture agrees well with the scattering and the collisional rearrangement process in the ion-atomic collision [35, 58]. As already mentioned, a nonlinear Compton type scattering with laser pulse is involved, as experimentally investigated by Meyerhofer et al. [54] and earlier in a theoretical work of Eberly et al. [38]. It is a collective scattering with the laser wave packet at high photon density or strong field, where the electron recoils or the electronic density is strongly polarized due to the strong electric field of the laser [23], similar to the ion-atom collision, as also discussed by Klaiber et al. [35]. Note, the effect caused by an electric field or a charge density is the same. According to Einstein, Wheeler and Feynman, electric charge and field are the same and not independent entities [59, 60].

In Fig. 6, we plot $\tau_{t ion}$ of eq 11 for $Z_{eff} = 1.6875$ (lower two curves) and $Z_{eff} = 1.344$ (higher two curves), where, for a better visibility, the curves correspond to $\Delta\nu = 0, 2$ are plotted. In Fig. 6, we included the result of the adiabatic case [1], see eq 3, with the experimental data of Landsman et al. [2]. This result may explain one of the reasons (intensity fluctuation), which causes the spread of the experimental points. It corresponds to the absorption of a slightly smaller number of photons than required by δ_z ($\bar{n}_F \lesssim n_F$) as shown in Figs 5, 6 and eq 11, although it is difficult to ensure such a conclusion since the error bars are larger than the separation between successive curves (or even between $\Delta\nu = 0, \Delta\nu = 2$). In addition, fig 6 suggests that the τ_{dion} curves (the nonadiabatic case) move towards $\tau_{T,d}$ curves, when $\Delta\nu \omega_0$ become larger, see eq 11, up to $\Delta\nu \omega_0 = \delta_z$ (the adiabatic case).

We come to the exit point in the case of eq 11. As discussed in sec. IV, it is in the range between x_m and x_E in the nonadiabatic case (no tunneling contribution). Whereas in the adiabatic case (adiabatic tunneling), it is estimated by $x_{e,+}$, compare Fig. 5. In the case of eq 11 (intermediate case), an approximate value can be obtained by the same procedure applied to obtain eqs 10, 11. The exit point shifts from x_m towards $x_{e,m1}, \dots, x_{e,mk}, \dots$ for $\Delta\nu = 1, \dots, k, \dots$, and reaches $x_{e,+}$ for $\Delta\nu \omega_0 = \nu_F \omega_0 \approx \delta_z$ (i.e. $\Delta\nu = \nu_F$ in eq 11). The barrier width changes in the same way. From the intersection points of the horizontal dashed lines (virtual states) with the effective potential curve, in Fig. 5, we find

$$d_B^\nu \approx \frac{\Delta\epsilon}{F} \approx \frac{\Delta\nu \omega_0}{F}, \quad (12)$$

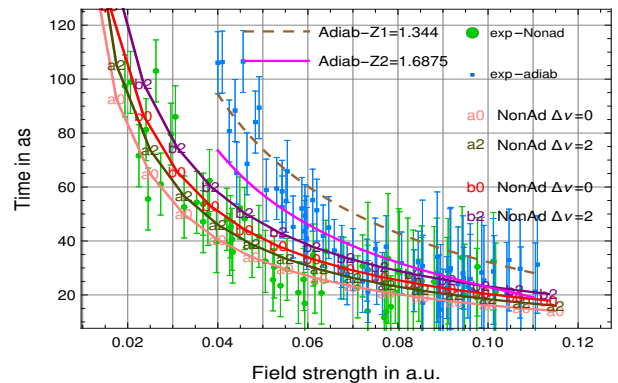


FIG. 6. (Color online) The figure shows the time delay $\tau_{t ion}$ given in eq 11 for $Z_{eff} = 1.6875$ and $\Delta\nu = 0, 2$ (lower two a-curves). And $Z_{eff} = 1.344$ and $\Delta\nu = 0, 2$ (upper two b-curves). The experimental data (blue, rectangles) with the adiabatic [2] and (green, circles) with nonadiabatic [20] field calibration. The two curves over the adiabatic experimental data are the T-time $\tau_{T,d}$ of eq 3 for $Z_{eff} = 1.6875$ (below, magenta), $Z_{eff} = 1.344$ (above, dashed light brown).

which becomes $d_B = \delta_z/F$ for $\Delta\nu = \nu_F$. We obtain the exit point (compare Fig. 5) approximately by,

$$x_{e,m,k} \approx x_m + \frac{d_B^\nu}{2} = \sqrt{\frac{Z_{eff}}{F}} + \frac{\Delta\epsilon}{2F} \quad (13)$$

Note, for $\Delta\nu = 0, \Delta\epsilon = 0$, we have $d_B^\nu = 0$ and $x_{em0} \equiv x_m$. In this case, the field-ionization happens along the vertical channel and the tunneling contribution is negligible, as already mentioned (light blue curve, the first dashed one below the effective potential curve in Fig. 5.) Therefore, as we have seen in eq 11 the second term in eq 13 indicates the tunneling contribution. The interesting case is tunneling near the top of the barrier, that is when $\Delta\epsilon$ is small enough ($\Delta\nu \sim 0, 1, 2$), where the tunneling probability is quite high, compare Fig. 5. In our view, the spread of the experimental points can be traced back to this issue. Furthermore, we see from eq 13 that the difference in the number of absorbed photons change the exit point from x_m to x_{em1}, x_{em2}, \dots toward $x_{e,+}$ (reaches x_E in between), which increases the time delay from the nonadiabatic case τ_{sym}, τ_{dion} for $\Delta\nu = 0$ (eq 7, 8) towards the adiabatic case $\tau_{T,d}$ for $\Delta\nu = \nu_F$ (eq 4 or 3).

Eq 11 can be rewritten in the form

$$\tau_{t ion}(F) = \frac{1}{2I_p} \frac{F_a}{F} \left(1 + \frac{\Delta\nu \omega_0}{I_p}\right) = \tau_a \frac{F_a}{F} \left(1 + \frac{\Delta\nu}{n_I}\right) \quad (14)$$

Eq 14 is important, since it is valid for the intermediate tunneling, but is independent of the laser frequency ω_0 . For $\Delta\nu = 0$, we have eqs 7, 8 (or the self-interference term in the Winful tunneling model, eq 5). It sets a limit from below to the time delay for the field-ionization, the nonadiabatic case, where only a negligible tunneling contribution exists (slightly below the barrier, the first dashed curve one from above, light blue, in Fig. 5.) The second term in eq 14 appears when $\Delta\nu > 0$, which is smaller than the first one and indicates a tunneling part, which increases the delay time up to the adiabatic case at $\Delta\nu = \nu_F$, or precisely at the (maximum) barrier height $\Delta\epsilon = \delta_z$.

In summary, after a first step or the scattering with the laser pulse, the multiphoton absorption (vertical channel) can be followed by (or co-exist with) a tunneling (horizontal channel, $\Delta\nu \neq 0$ in eq 11, 14), slightly below the top of the barrier, where the tunneling probability is notably high, compare Figs. 5, 6. The amount of this contribution is smaller than the error bars in the data of Hofmann et al. [20] (see Fig. 6). Therefore, in our view, a refinement on the experimental side could explain this issue much better. The

quantum lower limit is given by τ_a at $F = F_a$, ($\delta_z = 0$), where saturation is reached in $\tau_{T,d}$ for the adiabatic tunneling time, which explains the Hartman effect in quantum tunneling [27].

VI. CONCLUDING REMARKS

For more insight and a conclusive judgment to the issue, we discuss some points further in the following. As already noted, Klaiber et al. presented in [50], a result concerning the tunneling dynamics and the attoclock, by considering the experimental data of Boge et al. [40]. The Keldysh parameter in this work, $\gamma_K \sim 0.8-4.9$, is in the same range of the nonadiabatic field calibration of Hofmann et al. [20]. Klaiber et al. argued that the electron absorbs an effective number of photon \tilde{n} followed by a static tunneling at higher energy $E = -I_p + \tilde{n}\omega_0$ what they called a rule of thumb for the region $\gamma_K \lesssim 1$. The energy gain is defined semi-classically, with the assumption that $\tilde{n}\omega_0 = \delta\mathcal{E}$, where $\delta\mathcal{E}$ is an energy change during the under-the-barrier motion [50]. The rule is supposed to shift the exit point from the quasi-static exit point with $x_{e,qs} = I_p/F = x_C$ (Fig. 1) to the exit point $x_e = x_{e,qs} - \delta x$ (x_C is by no means correct, see sec. IV). The view of Klaiber et al. is shown in Fig. 5 by (orange) dashed-dotted curve with the exit point $x_{e,\tilde{n}}$ (compare with Fig. 1 of [50]). According to Klaiber et al. [50], in the "nonadiabatic" regime, the electron gains energy in the course of the under-the-barrier motion, the nonadiabatic corrections raise the energy level, and the tunnel exit shifts closer to the atomic core. In their work, they compared the emission angle of the most probable trajectory with the experimental data of Boge et al. [40] for He-atom.

To elucidate our discussion, we present Fig. 7, where we report our result with the experimental data of Hofmann et al. and include the experimental data of Boge et al. [40] and the result of Klaiber et al. (see Fig. 2 of [50]). We have to mention that both experimental results are from the same group at ETH Zurich, where the recent experimental result of Hofmann et al. [20] is supposed to be superior. To compare with our result the data of Boge et al. and Klaiber et al. have been converted from angle to time (in the same way as done by the Hofmann data). It is easy to see that the effective number of photons \tilde{n} assumed by Klaiber et al. have to be compared with our \tilde{n}_F . However, it easily to find that $\tilde{n} < \tilde{n}_F \lesssim n_F = \text{floor}(\delta_z/\omega_0)$, see text before eq 11 and Fig. 5. The tunneling step, which is supposed to occur after multiphoton absorption, is similar to that in our model. However, the better agreement of our result with the experimental data, as seen in Fig. 7, confirms our approach and our model as discussed in sec. II, III, V. The result of Klaiber et al. agrees well with the experimental data of Boge et al. [40], but its trend is not satisfactory. As already mentioned, the correct trend is determined (classically and quantum-mechanically) by the $\sim \frac{1}{F}$ dependency of the time delay, which can be inferred from the good agreement of our result with the experimental data, compare Figs 2, 3, 7.

Nevertheless, although Klaiber et al. [50] interpreting the time delay differently [50], we think that the agreement with our result indicates that the emission angle or equivalently, the time delay is caused by the barrier region (under-the-barrier motion by [50]) in contrast to the imaginary T-time picture, where the T-time is attributed to the tail of the atomic potential [5], although an equivalence between the two pictures can be established in the adiabatic case, as already discussed, and widely discussed in our previous works [1, 6, 22-24]. The comparison between the nonadiabatic and adiabatic case (of the field calibration) in Fig. 6, shows immediately that the increased time delay in the latter case is due to the barrier itself, the second term τ_{delt} in eq 4. Strictly speaking, it is eliminated by Hofmann's nonadiabatic field calibration. It affects a shift toward smaller field strength (increases the self-interference contribution from the Winful point of view, eq 5). Equivalently, for the same F, a time delay contribution in the adiabatic case emerges due to the second term τ_{delt} , the effects of the barrier it-

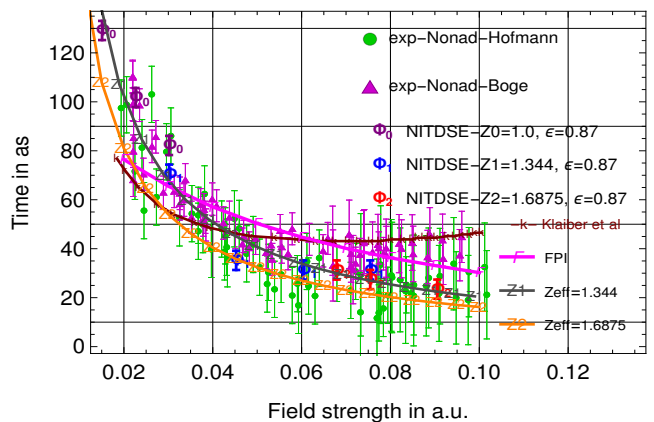


FIG. 7. (Color online) The figure shows the time delay τ_{tioon} given in eq 7 for $Z_{eff} = 1.6875$ and $Z_{eff} = 1.344$. As in figs 2, 3 the experimental data of Hofmann [20] (green circles) are shown, where we included the nonadiabatic experimental data (purple triangle) of Boge et al. [40] and the result of Klaiber et al. [50] (k, dark purple curve), see text. The NITDSE (see sec. A 1 and [26]), as in Fig. 3.

self. To conclude, if we compare eq 3 with eqs 7, 8 on one hand and the adiabatic with the nonadiabatic field calibration on the other hand, and then both with each other, we see that the field calibration maps ΔF to Δt (or $\Delta\theta$ of the streaking angle), which confirms the 'real' T-time picture (since δ_z is a real quantity). For $F \rightarrow 0$, we reach a maximal time delay Δt , that is $\lim_{F \rightarrow 0} \tau_{dion} = \infty$,

$\lim_{F \rightarrow 0} \delta_z = I_p, \tau_d \rightarrow \infty$. It is in accordance with the measurement of a closed system, intrinsic time and the uncertainty principle as discussed in [7] (for further discussion we kindly refer the reader to our previous works [1], [22] and [23].) We think that our conclusion is relevant for the theory of tunneling in general, especially that we found a relationship to the UTPP of Winful (compare eq 4 and eq 5), and to the Hartman effect or the Hartman paradox [27].

Finally, many experimental points (compare Fig. 6, 7) are below the limit of τ_{dion} ($\Delta\nu = 0, \Delta n = 0$ in eq 11, 10). This can not be explained this way. Since the use of SAEA or the Z_{eff} is not crucial as discussed in [20], it is difficult to understand this behavior. Multielectron effects are also small, they could be important for small barrier width, but hardly explain this behavior for a larger barrier width. Although the experiment is challenging, improvement is desirable. In particular, a refinement that reduces the spread of the experimental point and improving the error bars is useful to understand a tunneling contribution.

Conclusion In this work, we showed that our model is capable of describing the experimental result of the nonadiabatic field calibration of Hofmann et al. [20] for the attoclock, and we found a good agreement with the experimental data. Furthermore, we performed calculations of the NITDSE for the Z_{eff} used in our model, which strongly support our obtained result and our point of view. Particularly, in our nonadiabatic picture, multiphoton absorption is the most significant nonadiabatic effect. The time it takes at a field strength $F \leq F_a$, is a time delay with respect to the ionization at atomic field strength F_a , where the BSI sets up. The time delay generally consists of two terms. The first term, τ_{dion} (τ_{sym}), is solely because of $F < F_a$, and is it the time delay in the nonadiabatic field-ionization. The second term, τ_{delt} , is a time delay due to the barrier itself. It represents a tunneling contribution; it is largest in the adiabatic field calibration, for the maximum barrier height δ_z , which is discussed in previous work [1]. It saturates at the limit $F = F_a$, which explains the Hartman effect or Hartman paradox. Our view is in accordance with the UTPP of Winful [27]. We also discussed the intermediate regime especially right below

the top of the barrier, where the tunneling probability is notably high.

With this, we think that we have made an important contribution to resolving controversies related to the multiphoton and the tunneling regimes, since Keldysh parameter γ_K of eq 2 is usually not-strictly and vaguely applied in the strong-field regime. Also the use of so-called classical exit point x_C , as usually done, is by no mean a correct choice. The Keldysh parameter indicates two limiting cases tunneling and multiphoton regimes of the field-ionization, $\gamma_K \ll 1$, $\gamma_K \gg 1$, respectively. It is, however, mainly applied in the regime $\gamma_K \sim 1$ for the strong-field-ionization and in attosecond science.

Even if one insists on two different interpretations of the attoclock, nonadiabatic and adiabatic (which is important for the tunneling theory), the time it takes in both cases is a time delay with regard to the ionization at the atomic field strength F_a . It is in accordance with the intrinsic dynamical time point of view [1, 7, 24, 36]. Considering the experimental data of Hofman et al. [20] to present the correct calibration (apart from the error bars), the agreement presented in this work shows that after scattering with the laser pulse the traversing of the barrier region is essentially driven by multiphoton ionization, in strong field interaction. A tunneling contribution is possible, just below the top of the barrier and can be associated with an intermediate regime or intermediate tunneling, as discussed in sec. V. The attoclock receives a new boost, and the subtlety of the experimental investigations is more demanding than ever before. The investigation of the tunneling or tunnel-ionization in the future is essential to solve some of the questions regarding the tunneling process itself. The tunneling versus multiphoton ionization in the strong field, the attosecond, and the ultrafast science have become more challenging than ever.

Appendix A

1. Numerical Integration of the Time-Dependent Schrödinger Equation

We follow closely the numerical procedure we used to solve the TDSE in [26, 61]. We solve the TDSE for a single-electron atom with an effective central potential: $V(r) = -\frac{Z_{eff}}{r}$ in the presence of a laser pulse:

$$i\frac{\partial\Psi(\mathbf{r})}{\partial t} = (\hat{H}_{\text{atom}} + \hat{H}_{\text{int}}(t))\Psi(\mathbf{r}). \quad (\text{A1})$$

We use velocity form for the operator $\hat{H}_{\text{int}}(t)$ describing interaction of the atom with the laser field:

$$\hat{H}_{\text{int}}(t) = \mathbf{A}(t) \cdot \hat{\mathbf{p}}, \quad (\text{A2})$$

where $\mathbf{A}(t) = -\int_0^t \mathbf{E}(\tau) d\tau$ is the vector potential of the laser pulse, which for the geometry we employ (with quantization axis and pulse propagation direction along the z -axis), is defined as follows:

$$\begin{aligned} A_x(t) &= -\frac{f(t)}{\omega\sqrt{1+\epsilon^2}}F_0 \cos\omega t, \\ A_y(t) &= \frac{f(t)\epsilon}{\omega\sqrt{1+\epsilon^2}}F_0 \sin\omega t, \end{aligned} \quad (\text{A3})$$

where $\epsilon = 0.87$ is ellipticity of the pulse, F_0 its field strength (not to be confused with the *peak field strength* F which we use in the formulas in the main text). The function $f(t)$ in eq A3 is the pulse envelope which we chose as: $f(t) = \sin^{16}(\pi t/T_1)$, where $T_1 = 2T$, with $T = 2\pi/\omega$ - an optical cycle corresponding to the fundamental frequency $\omega = 0.062$ a.u., is a total duration of the pulse.

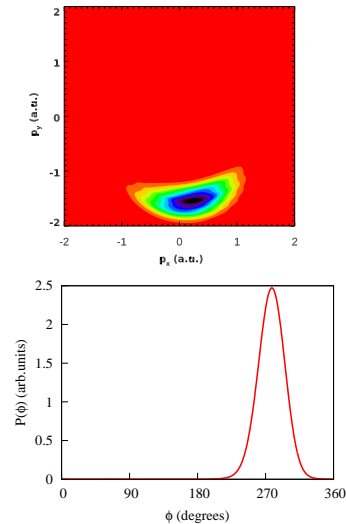


FIG. 8. Photo-electron momentum distribution in the polarization plane (above), and radially integrated distribution define by Eq A5 (below). Field and target parameters: $F_0 = 0.12$ a.u., $Z_{eff} = 1.6875$.

The initial state of the system is the ground $1s$ state of an atom with effective potential $V(r) = -\frac{Z_{eff}}{r}$. Solution of the TDSE is represented as a series in spherical harmonics:

$$\Psi(\mathbf{r}, t) = \sum_{l,m} f_l(r, t) Y_l^m(\theta, \phi), \quad (\text{A4})$$

where spherical harmonics with orders up to $L_{\text{max}} = 100$ were used for the highest field strength $F_0 = 0.12$ a.u. we employed in the calculations. The radial variable is treated by discretizing the TDSE on a grid with the step-size $\delta r = 0.1$ a.u. in a box of the size $R_{\text{max}} = 400$ a.u. Necessary checks were performed to ensure that for these values of the parameters L_{max} and R_{max} convergence of the calculations has been achieved. The wave-function $\Psi(\mathbf{r}, t)$ was propagated in time using the matrix iteration method [62].

Ionization amplitude into a photo-electron state with asymptotic momentum \mathbf{p} is computed by projecting the solution of the TDSE $\Psi(\mathbf{r}, T_1)$ at the end of the laser pulse on the scattering states $\phi_{\mathbf{p}}^-$ with ingoing boundary conditions.

We are interested in photo-electron momenta distribution $P(p_x, p_y, 0)$ in the polarization (p_x, p_y) -plane. A typical distribution we obtain using the procedure we described above is shown in Fig 8 (left) for $F_0 = 0.12$ a.u. and $Z_{eff} = 1.6875$. An observable we are after is the offset angle, which for the pulse defined by eq A3 is the angle between the negative y - direction and the ray pointing at the maximum of the photo-electron momentum distribution. To extract the offset angle, we follow the strategy we employed in [26]. We compute the radially integrated distribution $P(\phi)$ defined as:

$$P(\phi) = \int_0^\infty P(p_x, p_y, 0) p dp, \quad (\text{A5})$$

where $p = \sqrt{p_x^2 + p_y^2}$, factor p under the integral sign in eq A5 appears because of the area element in the (p_x, p_y) -plane, and angle ϕ is measured from the positive x - direction.

An example of the radially integrated distribution $P(\phi)$ is shown in Fig 8 (below). Offset angle now is determined as the location of the maximum of $P(\phi)$ minus 270 degrees.

Acknowledgments O. Kullie would like to thank C. Hofmann for sending the experimental data and FPI data shown in the figures, and R. Boge for forwarding the data presented in Fig 7, which was sent in the past when a previous work [23] was published. O. Kullie would like to thank Prof. Martin Garcia from the

-
- [1] O. Kullie, Phys. Rev. A **92**, 052118 (2015), arXiv:1505.03400v2.
- [2] A. S. Landsman, M. Weger, J. Maurer, R. Boge, A. Ludwig, S. Heuser, C. Cirelli, L. Gallmann, and U. Keller, Optica **1**, 343 (2014).
- [3] P. Eckle, A. N. Pfeiffer, C. Cirelli, A. Staudte, R. Dörner, H. G. Muller, M. Büttiker, and U. Keller, Science **322**, 1525 (2008).
- [4] P. Eckle, M. Smolarski, F. Schlup, J. Biegert, A. Staudte, M. Schöffler, H. G. Muller, R. Dörner, and U. Keller, Nat. Phys. **4**, 565 (2008).
- [5] U. S. Sainadh, H. Xu, X. Wang, Atia-Tul-Noor, W. C. Wallace, N. Douguet, A. W. Bray, I. Ivanov, K. Bartschat, A. Kheifets, R. T. Sang, and I. V. Litvinyuk, Nature **568**, 75 (2019), arxi.1707.05445 (2017).
- [6] O. Kullie, J. Phys. Commun. **2**, 065001 (2018).
- [7] Y. Aharonov and B. Reznik, Phys. Rev. Lett. **84**, 1368 (2000).
- [8] G. Auletta, M. Fortunato, and G. Parisi, *Quantum Mechanics* (Cambridge University Press, 2009).
- [9] V. S. Popov, Phys. of At. Nuclei **68**, 686 (2005).
- [10] A. M. Perelomov, V. S. Popov, and M. V. Terentév, Zh. eksp. teor. Fiz. **50**, 1393 (1966), [Soviet Phys. JETP, **23**, 924 (1966)].
- [11] S. V. Popruzhenko, J. Phys. B **47**, 204001 (2014).
- [12] M. Lewenstein, P. Balcou, M. Y. Ivanov, A. L’Huillier, and P. B. Corkum, Phys. Rev. A **49**, 2117 (1994).
- [13] S. Augst, D. Strickland, D. D. Meyerhofer, S. L. Chin, and J. H. Eberly, Phys. Rev. Lett. **63**, 2212 (1989).
- [14] S. Augst, D. D. Meyerhofer, D. Strickland, and S. L. Chin, J. Opt. Soc. Am. B **8**, 858 (1991).
- [15] M. Göppert-Mayer, Ann. of Phys. **401**, 273 (1931).
- [16] N. B. Delone and V. P. Kraĭnov, Phys.-Usp. **41**, 469 (1998).
- [17] L. V. Keldysh, Zh. eksp. teor. Fiz. **47**, 1945 (1964), [English translation: 1965, Soviet Phys. JETP, **20**, 1307].
- [18] F. H. M. Faisal, J. Phys. B **6**, L89 (1973).
- [19] H. R. Reiss, Phys. Rev. A **22**, 1786 (1980).
- [20] C. Hofmann, A. S. Landsman, and U. Keller, J. Mod. Opt. **66**, 1052 (2019), open access.
- [21] I. Y. Kiyan and V. P. Kraĭnov, Soviet Phys. JETP **73**, 429 (1991).
- [22] O. Kullie, Journal of Physics B: Atomic, Molecular and Optical Physics **49**, 095601 (2016).
- [23] O. Kullie, Ann. of Phys. **389**, 333 (2018), arXiv:1701.05012.
- [24] O. Kullie, Qunat. Rep. **2**, 233 (2020).
- [25] E. Clementi and D. L. Raimondi, J. Chem. Phys. **38**, 2686 (1963).
- [26] I. A. Ivanov and A. S. Keifets, Phys. Rev. A **89**, 021402 (2014).
- [27] H. G. Winful, Phys. Rev. Lett. **91**, 260401 (2003).
- [28] A. S. Landsman and U. Keller, Phys. Rep. **547**, 1 (2015).
- [29] N. B. Delone and V. P. Kraĭnov, *Multiphoton Processes in Atoms*, 2nd ed. (Springer-Verlag Berlin, 2000).
- [30] V. P. Majety and A. Scrinzi, J. Mod. Opt. **64**, 1026 (2017).
- [31] H. Ni, U. Saalman, and J. M. Rost, Phys. Rev. A **97**, 013426 (2018).
- [32] M. Y. Ivanov, M. Spanner, and O. Smirnova, J. Mod. Opt. **52**, 165 (2005).
- [33] F. H. M. Faisal, J. Phys. B **40**, F145 (2007).
- [34] F. H. M. Faisal, Phys. Rev. A **75**, 063412 (2007).
- [35] M. Klaiber and J. S. Briggs, Phys. Rev. A **94**, 053405 (2016).
- [36] P. Busch, in *Time in Quantum Mechanics - Vol. 1*, edited by J. G. Muga, R. S. Mayato, and I. L. Egusquiza, *Lecture Notes in Physics Vol. 734*, pp. 73–105 (Springer-Verlag, Berlin, 2008).
- [37] D. L. B. Sombillo and E. A. Galapon, Phys. Rev. A **97**, 062127 (2018).
- [38] J. H. Eberly, Phys. Rev. Lett. **15**, 91 (1965).
- [39] In previous works, O. Kullie used $Z_{eff} = 1.375 \approx \sqrt{2I_p} \approx 1.344$ from a model based on an unpublished thesis of him at the university of Kiel (Germany) for the He-atom, where the full screening of the first electron is accounted for. We still intend to expand the work for light rare gas atoms in the framework of the SAEA and publish it whenever possible.
- [40] R. Boge, C. Cirelli, A. S. Landsman, S. Heuser, A. Ludwig, J. Maurer, M. Weger, L. Gallmann, and U. Keller, Phys. Rev. Lett. **111**, 103003 (2013).
- [41] E. Yakaboylu, M. Klaiber, H. Bauke, K. Z. Hatsagortsyan, and C. H. Keitel, Phys. Rev. A **88**, 063421 (2013).
- [42] R. Ramos, D. Spierings, I. Racicot, and A. M. Steinberg, Nature **583**, 529 (2020).
- [43] M. Klaiber, K. Z. Hatsagortsyan, and C. H. Keitel, Phys. Rev. A **102**, 053105 (2020).
- [44] Y. H. Kim, I. A. Ivanov, and K. T. Kim, Phys. Rev. A **104**, 013116 (2021).
- [45] N. Douguet and K. Bartschat, Phys. Rev. A **97**, 013402 (2018).
- [46] L. Xu and L. B. Fu, Chin. Phys. Lett. **36**, 043202 (2020).
- [47] S. Yusofsani and M. Kolesik, Phys. Rev. A **101**, 052121 (2020).
- [48] D. B. Canário, M. Klaiber, and K. Z. Hatsagortsyan, arXiv.2208.10946 (2022), 10.48550/arXiv.2208.10946.
- [49] D. Trabert, N. Anders, S. Brennecke, M. S. Schöffler, T. Jahnke, L. P. H. Schmidt, M. Kunitski, M. Lein, R. Dörner, and S. Eckart, Phys. Rev. Lett. **127**, 273201 (2021).
- [50] M. Klaiber, K. Z. Hatsagortsyan, and C. H. Keitel, Phys. Rev. Lett. **114**, 083001 (2015).
- [51] U. S. Sainadh, R. T. Sang, and I. V. Litvinyuk, J. Phys. Photonics **2**, 042002 (2020).
- [52] H. Ni, U. Saalman, and J. M. Rost, Phys. Rev. A **98**, 013411 (2018).
- [53] C. Hofmann, private communication.
- [54] D. D. Meyerhofer, IEEE J. Quantum Electron. **33**, 1935 (1997).
- [55] O. Kullie, Mathematics **6**, 192 (2018).
- [56] H. Helm and M. J. Dyer, Phys. Rev. A **49**, 2726 (1994).

- [57] N. Camus, E. Yakaboylu, L. Fechner, M. Klaiber, M. Laux, Y. Mi, K. Z. Hatsagortsyan, T. Pfeifer, C. H. Keitel, and R. Moshhammer, *Phys. Rev. Lett.* **119**, 023201 (2017).
- [58] J. S. Briggs and J. H. Macek, *Adv. At. Mol. Opt. Phys.* **28**, 1 (1990).
- [59] C. Mead, *Collective Electrodynamics: Quantum Foundations of Electromagnetism* (MIT Press, Cambridge, Mass., 2000).
- [60] C. Mead, in *The Nature of Light: What are Photons? V*, Vol. 8832, edited by C. Roychoudhuri, A. F. Kracklauer, and H. D. Raedt, International Society for Optics and Photonics (SPIE, 2013) pp. 15 – 21.
- [61] I. A. Ivanov, J. Dubau, and K. T. Kim, *Phys. Rev. A* **94**, 033405 (2016).
- [62] M. Nurhuda and F. H. M. Faisal, *Phys. Rev. A* **60**, 3125 (1999).